

Bulk defect formations in KH_2PO_4 crystals investigated using fluorescence microscopy

S. G. Demos,* M. Staggs, and H. B. Radousky

Lawrence Livermore National Laboratory, PO Box 808, Livermore, California 94551, USA

(Received 22 July 2002; revised manuscript received 16 December 2002; published 6 June 2003)

Defect formations located in the bulk of KH_2PO_4 crystals are studied using a specially designed microscopic fluorescence imaging system. The concentration of the observed defect clusters varies depending on the crystal-growth method, the growth sector of the crystal, and the speed of growth. The experimental procedure involves acquisition of high-resolution fluorescence images of bulk defect cluster formations obtained under cw, 488-nm photoexcitation. Annihilation and/or passivation of these defects is observed under exposure of the crystal to high-power, 355-nm laser irradiation. This work suggests that native defects can influence the optical performance and characteristics of potassium dihydrogen phosphate.

DOI: 10.1103/PhysRevB.67.224102

PACS number(s): 61.72.Cc, 81.10.Aj, 42.70.-a

I. INTRODUCTION

KH_2PO_4 (potassium dihydrogen phosphate, or KDP is a transparent dielectric crystalline material that has extensively been incorporated into various laser systems for harmonic generation and electro-optic switching. The ability of KDP to grow at a fast rate (10–20 mm/day) and as large single crystals¹ has made it a suitable candidate for large-aperture laser systems. The optical performance of KDP (as well as that of its deuterated analog DKDP) is determined not only by its nonlinear optical characteristics but also by other considerations including its ability to preserve phase and polarization of the propagating laser beam and its resistance to laser-induced damage in high-power laser applications. The development of rapid crystal-growth methods for implementation in large-aperture lasers² requires preservation of high optical quality throughout the crystal plate, which can be as large as 50 cm or larger.

Since the beginning of the work on rapid growth of KDP crystals,^{1,3,4} an important point of concern has been the homogeneity associated with the presence of different growth sectors formed by {101} (pyramidal) and {100} (prismatic) faces that were affected differently by impurities.³ UV absorption is very sensitive to the amount of impurities, mainly trivalent metals incorporated into the crystal.^{5,6} Low levels of UV absorption is observed in the pyramidal growth sector, which increases on the sector boundary due to a higher absorption in the prismatic growth sectors.^{7–9} It was found that when the concentration of certain impurity ions such as chromium or iron was increased, the internal laser damage threshold decreased substantially.^{10,11} Damage testing experiments on KDP and DKDP crystals grown from solutions that contained various impurity concentrations demonstrated that for low impurity levels, the damage threshold remained unaffected by the impurity concentration.¹² This suggests that atomically dispersed impurity ions do not change the damage characteristics of the material and that clusters of impurities or crystal defects play a key role in damage initiation. It was also reported that increased dislocation density leads to an approximately linear decrease in the damage threshold.¹⁰

Beam propagation measurements in KDP crystals show that optical distortion is caused primarily by dislocations, differences in composition between adjacent growth sectors

of the crystal, and differences in composition between adjacent sectors of vicinal-growth hillocks within a single growth sector of the crystal.^{13–15} It was recently shown that striation formation in crystals can be caused not only by variations in external growth conditions, but also by the action of some internal factors such as variations in the dislocation structure of the crystal and modifications of the growth-step distribution on the growing faces.¹⁶

The role that native defects play in the optical characteristics and performance of KDP crystals has received less attention. A number of such defects have been identified using electron paramagnetic resonance (EPR) spectroscopy. Two distinct hole centers, the $[\text{HPO}_4]^-$ center (a hole trapped on an oxygen ion adjacent to a hydrogen vacancy) and the $[\text{H}_2\text{PO}_4]^0$ center (a hole shared by two oxygen ions) as well as interstitial hydrogen atoms that act as electron traps have been identified at low temperatures following irradiation of the sample with x rays or UV laser pulses.^{17–19} All these defects are unstable at room temperature. A transient absorption in the 350–600-nm spectral region that appears when KDP crystals are exposed to intense UV laser irradiation was assigned to the formation of short-lived $(\text{HPO}_4)^-$ centers.^{20,21} Resonance Raman-scattering spectroscopy experiments are supportive of this assignment,²² indicating that this defect plays an active role during high-power laser irradiation. Most recently, a hole trap and several electron traps that are stable at room temperature have been identified.²³ The hole is trapped on an oxygen ion adjacent to a silicon impurity. The electron is trapped at an oxygen vacancy, described as $(\text{PO}_3)^{2-}$ molecular ions, with a nearby cation vacancy (a missing proton or potassium). The silicon impurity was probably coming from the crystal-growth container. In addition, various impurities are found in the raw materials used in the crystal solution. Certain impurity ions are also intentionally introduced to improve the crystal properties or crystal-growth parameters (such as the aspect ratio between prism and pyramid sectors in fast-grown crystals¹). The presence of impurity defects can give rise to native defects for various reasons including charge compensation. Optical fluorescence microscopy has revealed the presence of defect formations in KDP at room temperature.²⁴ This technique was expanded to study *in situ* the reaction of indi-

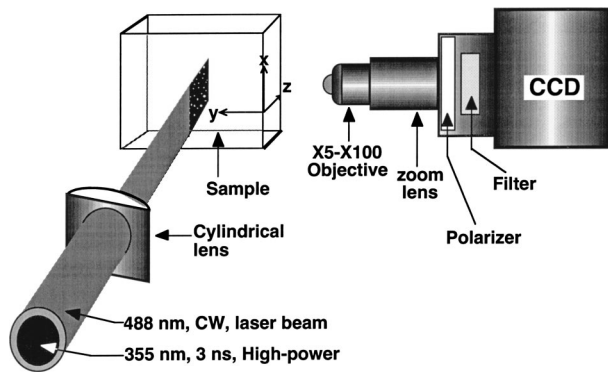


FIG. 1. Schematic diagram of the microscopic fluorescence imaging experimental setup.

vidual defect nanoclusters to high-power laser irradiation at 355 nm.²⁵

In this work, we utilize the fluorescence microscopy technique discussed in Refs. 24 and 25 to investigate the formation of native defect populations located in the bulk of KH_2PO_4 crystals near characteristic crystal-growth boundaries and their response to high-power laser irradiation. These defect formations can give rise to changes in the crystal parameters, inducing or contributing to a number of macroscopic effects such as laser damage, UV absorption, localized stress, and change of the index of refraction, which are currently attributed to different factors as discussed above.

II. EXPERIMENTAL SYSTEM

The experimental setup is shown in Fig. 1. The imaging system is composed of a microscope objective having magnification power of X10 followed by a X5 magnification lens system. The image was recorded using a liquid-nitrogen-cooled charge coupled device (CCD) detector. In this arrangement, $1 \mu\text{m}^2$ of an object at the image plane is projected and recorded on 1 pixel of the CCD. The imaging system was positioned along the y axis of the crystal and perpendicular to the direction of illumination. An argon laser operating at 488 nm was used as the source for photoexcitation of bulk defect formations. The resulting emission of these defects was used for the acquisition of the microscopic fluorescence images. The third harmonic (355 nm) of a 3-ns pulse width, Q-switched, Nd:yttrium aluminum garnet (YAG) laser was overlapped with the cw output of the argon laser to provide high-power illumination of the sample. The two overlapping and collimated beams were propagated along the z axis (optical axis) of the KDP crystal and focused inside the crystal using a 7.5-cm focal length cylindrical lens. The focal plane of the cylindrical lens that delivers the illumination beam into the sample is overlapped with the imaging plane of the microscope system. This configuration ensured that only fluorescing features located within the in-focus area of the microscope system were imaged and avoided an out-of-focus signal. The imaging depth was determined by the $\approx 25\text{-}\mu\text{m}$ depth of the illumination slit beam. An analyzer followed by a 640-nm long-wavelength-pass filter was positioned in front of the CCD detector. The analyzer

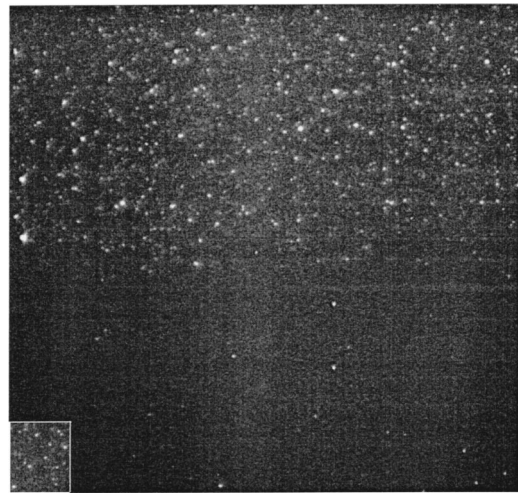


FIG. 2. Fluorescence image of a $430 \times 410 \times 25\text{-}\mu\text{m}^3$ section of a sample showing the boundary at which the crystal-growth speed was changed from 1 (lower part) to 8 mm/day (upper part). Inset in the lower left shows a $50 \times 110\text{-}\mu\text{m}^2$ section of the upper part of the image for comparison.

with its polarization vector parallel to the x axis was used in order to avoid image distortions due to the birefringence of the sample. The optical long-wavelength-pass filter was used in order to discriminate the fluorescence of defect centers from the Raman-scattering signal of the bulk. Additional information on the design and capabilities of the imaging system can be found in Refs. 24 and 25. The experiments were performed using KDP samples of various sizes that were cut in plates perpendicular to the c axis of the crystal. The crystals were grown at Lawrence Livermore National Laboratory using the fast-growth method. The samples studied were not intentionally exposed to any laser or other type of irradiation prior to this investigation. All experiments were carried out at room temperature.

III. EXPERIMENTAL RESULTS

Figure 2 presents the fluorescence image of a $430 \times 410\text{-}\mu\text{m}^2$ section in the bulk of a KDP crystal. It shows the presence of emission clusters located inside the bulk and a nearly uniform background emission. The sample was illuminated with $\approx 150\text{-mW}$, 488-nm, cw laser irradiation, using a 3-min exposure time of the CCD detector. The digitized intensity of the clusters varies, indicating that they represent an aggregation of individual defects. The growth parameters were changed during crystal growth and as a result, the speed of growth was changed. In the image shown in Fig. 2, the upper part of the crystal was grown at a speed of ≈ 8 mm/day while the lower part was grown at ≈ 1 mm/day. The fluorescence image in Fig. 2 clearly shows the boundary at which the growth parameters were changed. More specifically, the upper part of the image shows a higher number of emissive defect clusters (by a factor of ≈ 25) as well as a higher background emission intensity. This difference in background emission is best demonstrated by comparing the intensity of the lower part of the image to that of the image shown in the

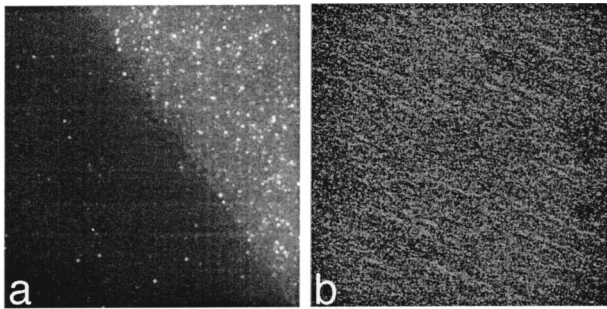


FIG. 3. Images of the same $190 \times 200 \times 25\text{-}\mu\text{m}^3$ section of the sample at the boundary between prismatic (lower-right) and pyramidal (upper-left) sectors using (a) our fluorescence microscopy system and 640-nm long-wavelength-pass filter and (b) a light-scattering image. Both images were obtained using 488-nm laser illumination.

inset in the lower left part of Fig. 2. The later image is from a $50 \times 110\text{-}\mu\text{m}^2$ section on the upper part of the image at which the speed of growth was greater.

Large differences in the concentration of the emission clusters were also observed on the sector boundary of fast-grown KDP crystals, allowing for a clear observation of the boundary. This is demonstrated in Fig. 3(a), where the fluorescence image of a $190 \times 200\text{-}\mu\text{m}^2$ section across the sector boundary of a fast-grown KDP crystal is shown. The sector boundary is oriented at 45° from the horizontal direction of the image plane with the prismatic sector located in the upper-right part of the image and the pyramidal sector in the lower-left part of the image. The concentration of the observed emission clusters in the prismatic (material grown on $\{100\}$ faces) sector was $\approx 3 \times 10^5$ per mm^3 while in the pyramidal (material grown on $\{101\}$ faces) sector it is reduced by a factor of 10. In addition to the characteristic defect clusters, the image shows the presence of a uniformly distributed background emission that is stronger in intensity in the prismatic sector. The light-scattering image of the same site of the sample is shown in Fig. 3(b). This image was obtained by replacing the 640-nm long-pass filter with a narrow-band interference filter at the operational wavelength (488 nm) of the laser. This image shows the presence of minimal scattering that does not correlate to the fluorescence image shown in Fig. 3(a). In the light-scattering image, the sector boundary is not visible and there is no clear difference in the scattering intensity from the two crystal sectors. In addition, there is nothing in the light-scattering map that can correspond to the observed emission clusters. This indicates that the emission clusters observed using fluorescence microscopy do not arise from structural defects but rather from electronic defects.

The images shown in Fig. 3 were obtained prior to any UV irradiation of the sample. The sample was thereafter illuminated with 355-nm pulses of average fluence of $\approx 1 \text{ J/cm}^2$ obtained from the Nd:YAG laser operating at a repetition rate of 100 Hz. Figures 4(a) and 4(b) show the fluorescence images obtained following 5 and 45 min, respectively, of irradiation of the same section of the sample with the 355-nm pulses. The later image shows a significant reduction

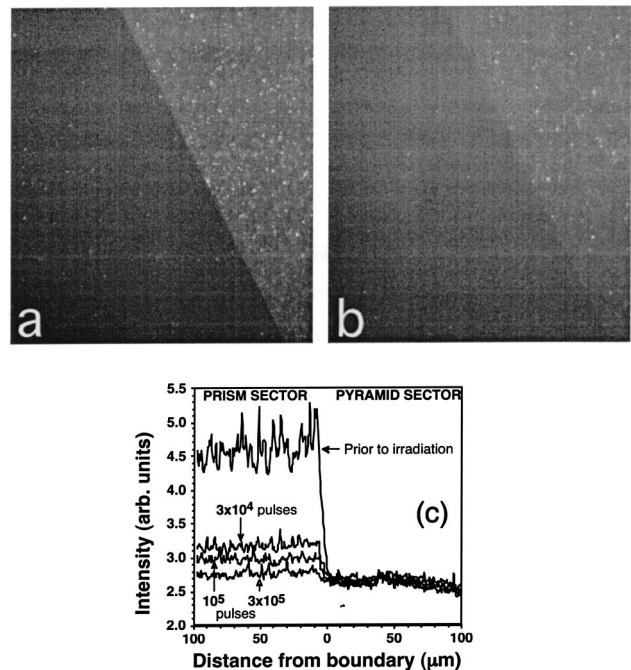


FIG. 4. A microscopic fluorescence image of a fast-grown KDP crystal at the sector boundary following (a) 5 min and (b) 45 min 355-nm irradiation with average fluence of $\approx 1 \text{ J/cm}^2$. (c) The digitized intensity profiles across a horizontal ten-pixel stripe at the middle of the images for different exposure times.

of the emission cluster concentration in both the prism and the pyramidal sectors. In addition, the intensity of the background emission is reduced. This is most pronounced in the prism sector, resulting in the reduction of the intensity difference between the two crystal sectors. This effect is better depicted in Fig. 4(c), which shows the sum of the digitized intensity profile of ten consecutive horizontal pixel lines at the middle of images obtained following exposure to $\approx 1 \text{ J/cm}^2$, 355-nm laser irradiation to different time intervals. Spikes in the digitized intensity are mainly due to the presence of defect clusters. These profiles demonstrate a “conditioning” effect that leads to an almost identical intensity level across the two crystal sectors. The conditioning effect observed in the prismatic sector occurs in the pyramidal sector as well but it is less intense due to the smaller emission cluster concentration and image intensity background. Figure 4(c) indicates that the main portion of the conditioning takes place in the initial ≥ 5 min of irradiation followed by a slower rate of conditioning.

The removal of the defect clusters from the area irradiated with 355-nm laser pulses demonstrated in Fig. 4 may be due either to their migration into the unirradiated part of the sample or to their annihilation and/or passivation. To address this question, the following experiment was performed. The sample was first imaged and then irradiated with 10^5 pulses at $\approx 1 \text{ J/cm}^2$ using a cylindrical lens to focus the 355-nm laser beam into the sample, with its focusing axis perpendicular to that of the cylindrical lens used to obtain the microscopic emission images. In this arrangement, only a small portion of the imaged part of the sample was exposed to the 355-nm pulsed irradiation. This emission image is shown in

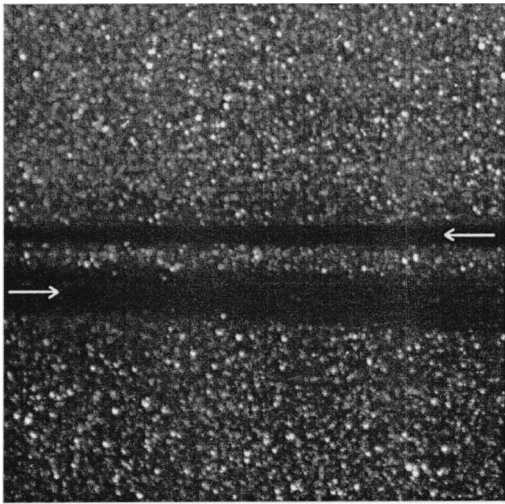


FIG. 5. Microscopic fluorescence image of a $600 \times 600 \times 25\text{-}\mu\text{m}^3$ section of the sample where a small portion (indicated with arrows) was irradiated with 10^5 , 355-nm pulses at $\approx 1\text{ J/cm}^2$.

Fig. 5. The 355-nm laser beam enters the sample from the right side of the image at the location indicated with an arrow, and the focal point of the beam is near the left side of the image. The beam propagates through the sample and when it reaches the output surface of the sample, ≈ 0.04 of its intensity is back-reflected and enters the imaged area of the sample from the left side. As seen in the image of Fig. 5, the irradiated areas of the sample have a much smaller defect density than that of the unirradiated areas. Most important, there is no additional concentration of defects near the irradiated zone, showing that their removal is not due to their migration but to their annihilation/passivation.

IV. DISCUSSION

The concentration of the observed emission clusters varies depending on the crystal-growth method, the sector of the crystal, and the speed of growth. In fast-grown crystals that were grown at a speed of $\approx 10\text{ mm/day}$, the defect cluster concentration in the prismatic sector was measured to be $\approx 3 \times 10^5\text{ per mm}^3$ while in the pyramidal sector it is $\approx 3 \times 10^4\text{ per mm}^3$. In the sample (prismatic sector) shown in Fig. 2, the concentration in the sections grown at a speed of $\approx 8\text{ mm/day}$ is $\approx 2.5 \times 10^5\text{ per mm}^3$, while in the part grown at $\approx 1\text{ mm/day}$ it is $\approx 1 \times 10^4\text{ per mm}^3$. It must be noted that the same defect clusters are observed on KDP crystals that were grown using the conventional method with a concentration on the order of $\approx 10^4\text{ per mm}^3$. In addition, the defect clusters are visible using laser excitation wavelengths of 351, 457, and 514 nm, indicating that their absorption spectrum is broad. The available experimental data (including optical and EPR spectroscopy) do not allow for an accurate identification of the defect species observed by fluorescence microscopy. The main problem is the low concentration of these defects in a material that it is known to contain various impurity ions incorporated during crystal growth. The emission spectrum arising from the defects observed using fluorescence microscopy has been shown in Ref. 24. This emission

may be interpreted as arising from defects with a blueshifted absorption spectrum similar or identical to that that gives rise to the transient absorption observed under intense 355- or 266-nm laser irradiation.^{20,21} As discussed above, this absorption has been assigned to the formation of an $(\text{HPO}_4)^-$ center. However, other types of defects may be present with an electronic structure that could support absorption under near-ultraviolet or visible laser irradiation. A theoretical study of the electronic structure of the various defects in KH_2PO_4 (currently in progress) indicates that interstitial hydrogen (H) in its neutral state leads to electronic states in the band gap that can be associated with absorption at low photon energies.²⁶ The addition or removal of an electron removes the H-induced states in the gap by forming strong bonds with its neighbor host H or O atoms, respectively. Similar results have been found for the case of interstitial hydrogen in silica.²⁷ States in the band gap of KDP are also found in the case of a positively charged hydrogen vacancy.

Our experimental results show that under laser irradiation, the number of defect clusters is continuously decreasing, depending on the laser fluence and exposure time. This decrease is observed on both the prism and the pyramid sector. A more detailed investigation of this effect has been discussed in Ref. 25, where we studied the behavior of individual defect nanoclusters under laser irradiation. This work showed that in response to irradiation by 3-ns laser pulses at 355 nm at subdamage threshold ($\approx 5\text{ J/cm}^2$) (visible-by-light-scattering-inspection alterations to the crystal integrity, referred to as laser damage, are observed in the same sample at an average fluence of $\approx 10\text{ J/cm}^2$) a segment of the defect cluster population exhibits sudden annihilation accompanied by a smaller number of new clusters that appears at different locations. This indicated that these defect clusters should be associated with transport of mobile electrons and/or holes. It is not possible that this effect can be produced by impurity ions because that would require unrealistic diffusion coefficients. The experimental results presented in Fig. 4 clearly show that the reduction of the defect cluster population is accompanied by reduction of background emission. This may be suggestive that the observed defect clusters represent aggregation of the same type of defects that contribute in part to the observed nearly uniform background emission. Such defect aggregations have been reported in similar systems.²⁸⁻³⁰ It is plausible that absorption of the laser light by the defect clusters is accompanied by energy loss through nonradiative relaxation that is initially distributed into the local vibrational modes associated with this defect formation.^{31,32} When a sufficient amount of laser energy is absorbed, overheating of the localized vibrational environment of the defect cluster may lead to its destabilization. The cluster can break apart and diffuse into a defect “continuum” composed of atomically dispersed defects of the same electronic origin. Following laser irradiation, the formation of a new aggregation of defects can lead to the appearance of new defect clusters. This process may continue for as long as laser light is absorbed. The experimental results shown in Fig. 5 indicate that this process is associated with annihilation or passivation through the generation of new defect

structures that do not absorb the 355-nm irradiation. A typical example of such a defect passivation process (and a possible explanation of what causes the laser conditioning effect) is in the case of the interstitial hydrogen defect (discussed above), which gives rise to H-induced states in the band gap that can be eliminated with the addition or removal of an electron.²⁶

It has been reported previously that 355-nm pulsed laser illumination of KDP crystals at subdamage laser threshold intensities leads to an increased laser-induced damage threshold³³ (laser annealing or conditioning). More recently, similar experiments have demonstrated that laser annealing raises the damage threshold of KDP and DKDP crystals for laser operation at 1064 and 355 nm.³⁴ The damage sites are generally smaller and the density of their formation at particular laser fluences is reduced in the conditioned regions of the same crystal. Furthermore, thermal annealing (exposure of the sample to temperatures below the tetragonal/monoclinic phase transition at about 180 °C) leads to an increase of the damage threshold at 1064 but not at 355 nm.^{33–35} Figure 4(b) shows a dramatic change in the defect concentration that could be described as laser annealing. We have not yet demonstrated a direct correlation of the observed defect formations with laser-induced damage in KDP. However, their presence may contribute to laser-induced heating, enhancement of absorption, lowering of nonlinear optical performance, and damage to the crystal. We have also performed thermal annealing experiments and we were not able to detect a measurable change in the defect formations (change in intensity or concentration of defect clusters) using our fluorescence microscopy system.

This work suggests that impurity ions may not be the only contributors to the absorption observed in the UV spectral region in the KDP crystal.^{5,6,12} Native defects can also give rise to absorption in the UV spectral region and contribute to the spectrum. This is supported by measurements of the UV absorption in samples that were exposed to laser irradiation.^{36,37} These experiments have shown that the UV absorption spectrum changes, usually leading to reduced absorption following irradiation with near-UV laser irradiation. This is consistent with the observed reduction of the defect population following 355-nm laser irradiation as shown in Figs. 4 and 5.

X-ray topographic imaging has demonstrated that the lattice parameters in the crystal section corresponding to the slow growth rate are slightly different, compared with the areas of the crystal grown at higher growth rates.¹⁶ This effect, as well as optical distortion effects, have also been assigned, to a large extent, to compositional heterogeneity arising from different incorporation of impurities.¹³ The compositional heterogeneity causes spatial variations in the refractive index and induces a distortion of the transmitted-wave front, while large groups of dislocations are respon-

sible for strain-induced birefringence that leads to beam depolarization. X-ray topography methods qualitatively show that the lattice parameters of a crystal are different in different vicinal sectors. This effect has also been assigned to the nonuniform stoichiometric composition or the incorporation of impurities into various vicinal sectors on the crystal faces^{14,15} while native defects have been overlooked. The experimental results shown in Figs. 2 and 3 demonstrate that these regions of the crystal (such as sector boundaries) that give rise to the aforementioned effects exhibit a very different population of optically active native defects observed using fluorescence microscopy. Since the presence of a large defect population can lead to a change in lattice constants, it may be important to reconsider the role these defects can play in the generation of the macroscopic crystal performance issues discussed above.

It is well documented that impurities incorporate in different crystal sectors at different rates.³⁸ It is likely that the defects observed in this work represent a mechanism during crystal growth for compensating for the incorporation of impurities. However, native defects can also lead to additional effects that have not yet been documented for the case of KDP crystals. For example, in the device-processing literature for silicon integrated circuits it has been well documented that an excess of vacancies results in enhanced diffusion.^{30,39} Such effects may play a role in the aging process of KDP or DKDP crystals at the sector boundaries or near the surface by increasing the mobility of impurity or stoichiometric ions. Recent observations of DKDP surface cracking have been attributed to the presence of vacancies leading to hydrogen diffusion into the crystal. A tensile surface layer results, due to a decrease in the equilibrium (100) lattice constant with increased H content.⁴⁰

V. CONCLUSION

Optically active defect formations located in the bulk of KDP crystals were studied using fluorescence microscopy. It was found that the observed defect concentration depends on the growth conditions and that it correlates to known optical properties and characteristics of the material. This work suggests that native defects can play an important role in the quality and performance of the material.

ACKNOWLEDGMENTS

We thank Dr. N. P. Zaitseva for providing some of the samples and for useful discussions. This work was performed under the auspices of the U.S. Department of Energy by the University of California Lawrence Livermore National Laboratory under Contract No. W-7405-Eng-48 through the Institute for Laser Science and Applications and the Materials Research Institute.

*FAX: (925) 423-2463.

¹N. P. Zaitseva, J. J. De Yoreo, M. R. Dehaven, R. L. Vital, K. E. Montgomery, M. Richardson, and L. J. Atherton, *J. Cryst. Growth* **180**, 255 (1997).

²E. M. Campbell, *Fusion Technol.* **26**, 755 (1994).

³L. N. Rashkovich, *KDP Family of Crystals* (Hilger, London, 1991).

⁴N. P. Zaitseva, I. L. Smol'sky, and L. N. Rashkovich, *Kristal-*

- lografiya **36**, 198 (1991) [Sov. Phys. Crystallogr. **36**, 113 (1991)].
- ⁵E. Diequez, A. Cintas, P. Hernandez, and J. Cabrera, *J. Cryst. Growth* **73**, 193 (1985).
- ⁶V. I. Bredikhin, N. V. Kiseleva, and V. V. Korolikhin, *Inorg. Mater. (Transl. of Neorg. Mater.)* **22**, 94 (1986).
- ⁷T. Amandosov, Z. S. Pashina, and L. N. Rashkovich, *Kvant. Elektron. (Moscow)* **10**, 469 (1983) [Sov. J. Quantum Electron. **13**, 271 (1983)].
- ⁸P. Lokshin, *Crystallogr. Rep.* **41**, 1061 (1996).
- ⁹K. Fujioka, S. Matsuo, T. Kanabe, H. Fujita, and M. Nakatsuka, *J. Cryst. Growth* **181**, 265 (1997).
- ¹⁰G. Endert and M. L. Martin, *Cryst. Res. Technol.* **16**, K65 (1981).
- ¹¹V. V. Azarov, L. V. Atroshchenko, Yu. K. Danileiko, M. I. Kolybaeva, Yu. P. Minaev, V. N. Nikolaev, A. V. Sidorin, and B. I. Zakharkin, *Kvant. Elektron. (Moscow)* **12**, 151 (1985) [Sov. J. Quantum Electron. **15**, 89 (1985)].
- ¹²A. K. Burnham, M. Runkel, R. A. Hawley-Fedder, M. L. Carman, R. A. Torres, and P. K. Whitman, *Proc. SPIE* **4347**, 373 (2002), and reference therein.
- ¹³J. J. De Yoreo, Z. U. Rek, N. P. Zaitseva, and B. W. Woods, *J. Cryst. Growth* **166**, 291 (1996).
- ¹⁴A. A. Chernov, *Modern Crystallography*, 1st ed., edited by B. K. Vainstein, A. A. Chernov, and L. A. Shuvalov (Springer, Berlin, 1984), Vol. 3, Chap. 1, pp. 7–232.
- ¹⁵I. L. Smolsky, A. A. Chernov, Yu. G. Kuznetsov, V. F. Parnov, and V. N. Rozhanskii, *Kristallografiya* **30**, 971 (1985) [Sov. Phys. Crystallogr. **30**, 563 (1985)].
- ¹⁶I. L. Smolsky, A. E. Voloshin, N. P. Zaitseva, E. B. Rudneva, and H. Klapper, *Philos. Trans. R. Soc. London, Ser. A* **357**, 2631 (1999).
- ¹⁷R. C. DuVarney and R. P. Kohin, *Phys. Rev. Lett.* **20**, 259 (1968).
- ¹⁸E. Diequez, J. M. Cabrera, and F. Agullo-Lopez, *J. Chem. Phys.* **81**, 3369 (1984).
- ¹⁹S. D. Setzler, K. T. Stevens, L. E. Halliburton, M. Yan, N. P. Zaitseva, and J. J. De Yoreo, *Phys. Rev. B* **57**, 2643 (1998).
- ²⁰J. E. Davis, R. S. Hughes Jr., and H. W. H. Lee, *Chem. Phys. Lett.* **207**, 540 (1993).
- ²¹C. D. Marshall, S. A. Payne, M. A. Hensian, J. A. Speth, and H. T. Powell, *J. Opt. Soc. Am. B* **11**, 774 (1994).
- ²²S. G. Demos, M. Yan, M. Staggs, J. J. De Yoreo, and H. B. Radousky, *Appl. Phys. Lett.* **72**, 2367 (1998).
- ²³N. Y. Garces, K. T. Stevens, L. E. Halliburton, S. G. Demos, H. B. Radousky, and N. P. Zaitseva, *J. Appl. Phys.* **89**, 47 (2001).
- ²⁴S. G. Demos, M. Staggs, M. Yan, H. B. Radousky, and J. J. De Yoreo, *Opt. Lett.* **24**, 268 (1999).
- ²⁵S. G. Demos, M. Staggs, H. B. Radousky, and J. J. De Yoreo, *Opt. Lett.* **26**, 1975 (2001).
- ²⁶C. S. Liu, Nicholas Kioussis, S. G. Demos, and H. B. Radousky, *Phys. Rev. Lett.* (to be published).
- ²⁷A. Yokozawa and Y. Miyamoto, *Phys. Rev. B* **55**, 13 783 (1997).
- ²⁸A. V. Gektin, V. Y. Serebryanny, and N. V. Shiran, *Phys. Status Solidi A* **134**, 351 (1992).
- ²⁹E. Kotomin, M. Zaiser, and W. Soppe, *Philos. Mag. A* **70**, 313 (1994), and references therein.
- ³⁰G. H. Gilmer, T. Diaz de la Rubia, D. M. Stock, and M. Jaraiz, *Nucl. Instrum. Methods Phys. Res. B* **102**, 247 (1995).
- ³¹Dana M. Calistru, S. G. Demos, and R. R. Alfano, *Phys. Rev. Lett.* **78**, 374 (1997).
- ³²S. G. Demos, Dana M. Calistru, S. Owen, V. Petricevic, and R. R. Alfano, *Phys. Rev. Lett.* **82**, 2556 (1999).
- ³³J. Swain, S. Stokowski, D. Milam, and F. Rainer, *Appl. Phys. Lett.* **40**, 350 (1982).
- ³⁴L. J. Atherton, F. Rainer, J. J. De Yoreo, I. M. Thomas, N. Zaitseva, and F. De Marco, *Proc. SPIE* **2114**, 36 (1994).
- ³⁵V. V. Azarov, L. V. Atroshchenko, M. I. Kolybaeva, E. N. Leonova, and S. M. Selin, *Inorg. Mater. (Transl. of Neorg. Mater.)* **19**, 147 (1983).
- ³⁶H. Gong, Y. Sun, and C. Li, *Proc. SPIE* **3578**, 516 (1999).
- ³⁷M. Runkel, K. Neeb, M. Staggs, J. Auerbach, and A. Burnham, *Proc. SPIE* **4679**, 368 (2002).
- ³⁸Zaitseva, L. Carman, I. Smolsky, R. Torres, and M. Yan, *J. Cryst. Growth* **204**, 512 (1999), and reference therein.
- ³⁹M. Fahey, P. B. Griffin, and J. D. Plummer, *Rev. Mod. Phys.* **61**, 289 (1989).
- ⁴⁰George Gilmer, Chris Krenn, Terry Land, Tayyab Suratwala, Alan Burnham, and Tomas Diaz de la Rubia, Lawrence Livermore National Laboratory, Report No. NIF 0077324 (unpublished).